Passivity-Based Stabilization of Underwater Gliders With a Control Surface[1]

Feitian Zhang
Collective Dynamics and Control Lab,
Department of Aerospace Engineering,
University of Maryland,
College Park, MD 20742
e-mail: fzhang17@umd.edu

Xiaobo Tan[2]
Smart Microsystems Lab,
Department of Electrical
and Computer Engineering,
Michigan State University,
East Lansing, MI 48823
e-mail: xbtan@msu.edu

The problem of stabilizing steady gliding is critical for an underwater glider, which is subject to many non-negligible disturbances from the aquatic environment. In this paper, we propose a new systematic controller design and implementation approach for the stabilization problem, including a nonlinear, passivity-based controller and a nonlinear model-based observer, where the actuation is realized through a whale tail-like control surface. The controller is designed based on an approximation of a reduced model that is obtained through singular perturbation analysis, and consequently, it does not require full state feedback. The local stability of the full closed-loop system is established through linearization analysis. The nonlinear observer is designed to estimate the velocity-related system states, which are difficult to measure for such low-speed underwater vehicles. Simulation results are first provided to demonstrate that the proposed controller achieves rapid convergence in stabilization and the proposed observer has good performance especially in robustness against measurement noise. Experimental results using a gliding robotic fish are presented to support the effectiveness of both the controller and the observer. [DOI: 10.1115/1.4029078]

1 Introduction

There is a growing interest in monitoring aquatic environments with underwater vehicles and robots. Different types of sensing platforms are being developed. Among them, underwater gliders [1] have demonstrated extraordinary energy-efficiency and long-duration operation. An underwater glider utilizes its buoyancy and gravity to enable motion without any additional propulsion. At the same time, it adjusts its center of gravity to achieve certain attitude, which results in glide and thus horizontal travel. Since energy is needed only for buoyancy and center-of-gravity adjustment when switching the glide profile, underwater gliders are very energy-efficient, as proven by the great success of the Seaglider [2], Spray [3], and Slocum [4], the first generation of underwater gliders.

For most of its operation time, an underwater glider holds a preset steady gliding path without any energy consumption [5]. The gliding angle is calculated before deployment so that the glider will follow a designed trajectory, which either minimizes the energy cost or maximizes the field mapping ability [6]. However, an underwater glider is subject to many non-negligible uncertainties from the aquatic environment (e.g., current disturbance), which result in additional energy cost because counteracting the deviation from the preset course requires recalibration and control effort to keep the glider on or bring it back to the designed path [7–9]. The stability property of the steady gliding path and fast convergence to the path, are important for an underwater glider or any other buoyancy-driven underwater robot in reducing the energy expenditure on path correction, especially when they operate in shallow waters, such as lakes and rivers.

There are some stabilization control methods discussed in the literature. Most of them use the net buoyancy and internal mass displacement as control variables. For instance, in Refs. [10] and [11], the authors presented an linear quadratic regulator (LQR) controller and a proportional-integral-derivative (PID) controller, respectively, based on linearized models. Although in the LQR method energy is used as a cost function, the approach does not consider the additional cost for the course correction and guidance. Nonlinear controllers involving torque control and buoyancy control are proposed in Ref. [12], but those methods require full state feedback for the controller implementation, which will increase the complexity of the software and hardware. A Lyapunov-based control design is reported in Ref. [13]; however, using both elevator control and buoyancy control, it only deals with an open-loop control strategy with fixed-value control input to achieve a certain equilibrium gliding path.

Regarding controller implementation, while most reported control methods require the velocity-related state feedback [10–13], those variables are often unavailable for underwater robots. The most commonly adopted underwater velocity sensors are pitometer logs that use pressure difference information, and acoustic Doppler velocity logs that use Doppler effect of sound waves [14,15]. The cost of tens of thousands of dollars required for such sensors and their large sizes make it difficult to adopt them in underwater gliders. In addition, the accuracy of velocity sensing is usually low in the range of slow speeds (typically <0.5 m/s) that an underwater glider operates at. There are only limited discussions in the literature about using a linear observer to estimate the unknown velocity-related states [10]. Although the simplicity of a linear observer is desirable, the noise in the sensor measurements, like those in the Euler angles computed from data provided by an inertial measurement unit (IMU), will limit the working region of the linear observer to a small neighborhood of the equilibrium point. Finally, the discussion in the literature on the performances of those reported controllers in experimental implementation has been limited.

In this paper, we present a new, passivity-based nonlinear controller for the stabilization of an underwater glider. We focus on the stabilization problem using only a control surface, e.g., an elevator for an underwater glider. Compared to controlling the dynamics of net buoyancy and internal mass displacement, manipulating the dynamics of a control surface is more convenient and the resulting dynamic response is faster, which facilitates the

[1]This paper was written when Feitian Zhang was a Ph.D. student at Michigan State University.

[2]Corresponding author.

Contributed by the Dynamic Systems Division of ASME for publication in the Journal of Dynamic Systems, Measurement, and Control. Manuscript received April 27, 2014; final manuscript received November 5, 2014; published online January 27, 2015. Assoc. Editor: Hashem Ashrafiuon.

stabilization of an underwater glider. We utilize some singular perturbation results from [13], to reduce the full-order system to a second-order system. Then we propose a passivity-based controller using an approximation to the reduced system. We apply this controller, which is based on the reduced state information and easy to implement, to the original full-order system. Through linearization and singular perturbation analysis, we establish that, with sufficient time-scale separation, the equilibrium gliding path for the full-order closed-loop system is locally stable. Simulation results are presented to illustrate the proposed method, which demonstrates fast convergence speed. To solve the problem of velocity-related state estimation, we propose a model-based nonlinear observer to estimate those unknown system states using only the information of the pitch angle, which can be computed from onboard IMU data with relatively high accuracy and consistency. Lyapunov analysis is used to show the convergence of the proposed observer dynamics. The nonlinear observer proves to have satisfying performance in simulation, especially in terms of its robustness against the measurement noise.

The proposed controller and observer are further evaluated experimentally with a novel underwater robot called gliding robotic fish [16]. The robot is a hybrid of an underwater glider and a tail-actuated robotic fish. In the experiments, the tail is configured like a whale fluke to stabilize the gliding. We first run open-loop experiments to confirm the effectiveness of the nonlinear observer. The proposed nonlinear observer is then implemented in the passivity-based stabilization controller, which demonstrates effectiveness in stabilizing the glide trajectory to a preset profile following a significant perturbation. Stabilization experiments using P/PI controllers are also conducted as a comparison. The experimental results show that the proposed passivity-based controller has better overall performance, especially in terms of the balance between convergence speed and control effort.

The remainder of the paper is organized as follows: In Sec. 2, we review the dynamic model in the sagittal plane for the underwater glider, and separate it into the slow dynamics and fast dynamics based on singular perturbation analysis. In Sec. 3, we propose a passivity-based nonlinear controller for the approximated reduced model, and conduct stability analysis for the full system via linearization. Then simulation results are presented to show the effectiveness of the proposed controller. A nonlinear observer is proposed in Sec. 4 for implementation of the designed passivity-based controller. In Sec. 5, we present both open-loop and closed-loop experimental results using a gliding robotic fish to illustrate the effectiveness of both the controller and the observer. Finally, concluding remarks are provided in Sec. 6. A preliminary version of some results in this paper was presented at the 2012 American Control Conference [17], which was focused only on the passivity-based control design; enhancements in this paper include both the design of the nonlinear observer and the experimental validation of the controller and observer.

2 Model of an Underwater Glider

In this section, we first review a dynamic model for underwater gliders in the sagittal plane [13,17], which is an invariant plane for such gliders. Then, with singular perturbation analysis, the model is separated into two subsystems, a fast-mode system and a slow-mode system, for controller design in Sec. 3.

2.1 Dynamic Model in the Sagittal Plane. In this paper, we focus on the motion in the glider's invariant plane. As shown in Fig. 1, an underwater glider is modeled as a rigid-body system, with an ellipsoidal shape and fixed wings as typically reported in the underwater glider literature. The relevant coordinate reference frames are defined as follows: the body-fixed reference frame, denoted as $Ox_by_bz_b$, has its origin O at the geometric center. The Ox_b axis is along the body's longitudinal axis pointing to the head; the Oz_b axis is perpendicular to Ox_b axis in the sagittal plane

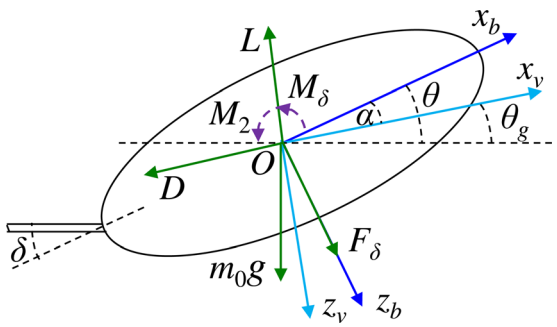

Fig. 1 The schematic of an underwater glider with forces and moments defined in the corresponding coordinate frames (side view)

of the glider pointing downwards, and Oy_b axis will be automatically formed by the right-hand orthonormal principle. In the velocity reference frame $Ox_vy_vz_v$, Ox_v axis is along the direction of velocity whose magnitude is V, and Oz_v lies in the sagittal plane perpendicular to Ox_v. In the inertial frame $Axyz$ (not shown in Fig. 1), Az axis points in the gravitational acceleration direction, and Ax is defined in the same direction as the intersection line of the horizontal plane and the sagittal plane, while the origin A is a fixed point in space. There are three angles defined following the standard convention in marine applications, based on the aforementioned reference frames. The pitch angle θ is the angle between Ox_b and Ax with nose up as positive; the gliding angle θ_g is the angle between Ox_v and Ax with gliding up as positive; the angle of attack α is the angle from Ox_b axis to Ox_v axis with rotation axis Oy_b.

We define the sum of the mass of the glider, m_g, and the added mass in Ox_b direction as m_1, and similarly, the sum of m_g and the added mass in Oz_b direction as m_3. The glider displaces a volume of water of mass m_w. Let $m_0 = m_g - m_w$ represent the excess mass (negative buoyancy).

The forces acting on the glider body include gravitational force, buoyancy force, hydrodynamic forces (lift and drag), and control force. Due to the symmetric shape of the glider, the center of buoyancy will be through the origin O. We take assumptions as in Ref. [13], that the movable mass is fixed at the origin O (during steady gliding), with the stationary mass distributed uniformly, and the added masses are equally valued ($m_1 = m_3 = m$). Then, the center of gravity will coincide with the center of buoyancy at the origin. The force pair, gravitational force and buoyancy force, acts like one force of excess mass m_0 at the origin O in Az direction. The hydrodynamic lift force L is along negative Oz_v axis, while the drag force D is along negative Ox_v direction. The control force F_δ is in Oz_b direction, exerted by the control surface (e.g., an elevator or whale fluke-type tail) traveling through the fluid medium, which is essentially another hydrodynamic force. The control surface angle δ is defined as the angle between the control surface plane and the Ox_by_b plane. The hydrodynamic forces are dependent on the angle of attack and the velocity as follows:

$$L = (K_{L0} + K_L\alpha)V^2 \tag{1}$$

$$D = \left(K_{D0} + K_D\alpha^2\right)V^2 \tag{2}$$

$$F_\delta = K_{F_\delta}V^2u_\delta \tag{3}$$

where K_{L0}, K_L are lift coefficients and K_{D0}, K_D are drag coefficients. u_δ is the effective angle of attack that the control surface contributes to the glider. There is a linear relationship between u_δ and the control surface angle δ, $u_\delta = K_{u_\delta}\delta$, where K_{u_δ} is a scale constant. K_{F_δ} is the coupling factor that describes the additional force that the control surface induces.

There are two moments about the Oy_b axis, which rotate the glider to a specific attitude. One is the hydrodynamic pitch moment M_2, and the other is the control moment M_δ. They are modeled as

$$M_2 = (K_{M0} + K_M\alpha + K_{q2}\omega_2)V^2 \tag{4}$$

$$M_\delta = -K_M u_\delta V^2 \tag{5}$$

where K_{M0} and K_M are pitch moment coefficients, K_q is the pitching damping coefficient, and ω_2 is the angular velocity for the pitch.

By applying Newton's second law and the moment of momentum equation, we obtain the glider dynamics as

$$\dot{V} = -\frac{1}{m_1}(m_0 g \sin\theta_g + D - F_\delta \sin\alpha) \tag{6}$$

$$\dot{\theta}_g = \frac{1}{m_1 V}(-m_0 g \cos\theta_g + L + F_\delta \cos\alpha) \tag{7}$$

$$\dot{\alpha} = \omega_2 - \frac{1}{m_1 V}(-m_0 g \cos\theta_g + L + F_\delta \cos\alpha) \tag{8}$$

$$\dot{\omega}_2 = \frac{1}{J_2}(K_{M0} + K_M\alpha + K_{q2}\omega_2 - K_M u_\delta)V^2 \tag{9}$$

where J_2 is the total inertia about Oy_b axis, consisting of stationary mass inertia and added inertia in water, and g represents the gravitational acceleration.

For the open-loop system (i.e., $u_\delta = 0$), the steady gliding profile can be obtained from Eqs. (6)–(9). The state variables at the equilibrium have the following relationships:

$$\theta_{g_e} = \arctan\frac{-K_{D_e}}{K_{L_e}}, \quad \alpha_e = -\frac{K_{M0}}{K_M},$$

$$\omega_{2e} = 0, \quad V_e = \left(\frac{|m_0|g}{\sqrt{K_{D_e}^2 + K_{L_e}^2}}\right)^{\frac{1}{2}}$$

where $K_{D_e} = K_{D0} + K_D\alpha_e^2, K_{L_e} = K_{L0} + K_L\alpha_e$.

2.2 System Reduction Via Singular Perturbation. Bhatta and Leonard [13] have shown with singular perturbation analysis that for the open-loop system, the dynamic model can be reduced to a second-order system with good approximation, and the corresponding nondimensional full state model is

$$\frac{d\bar{V}}{dt_n} = -\frac{1}{K_{D_e}V_e^2}(m_0 g \sin(\bar{\theta}_g + \theta_{g_e}) + D - F_\delta \sin(\bar{\alpha} + \alpha_e)) \tag{10}$$

$$\frac{d\bar{\theta}_g}{dt_n} = \frac{1}{K_{D_e}V_e^2(1+\bar{V})}(-m_0 g \cos(\bar{\theta}_g + \theta_{g_e}) + L + F_\delta \cos(\bar{\alpha} + \alpha_e)) \tag{11}$$

$$\varepsilon_1\frac{d\bar{\alpha}}{dt_n} = \bar{\omega}_2 - \varepsilon_1\frac{1}{K_{D_e}V_e^2(1+\bar{V})}(-m_0 g \cos(\bar{\theta}_g + \theta_{g_e}) + L + F_\delta \cos(\bar{\alpha} + \alpha_e)) \tag{12}$$

$$\varepsilon_2\frac{d\bar{\omega}_2}{dt_n} = -(\bar{\alpha} + \bar{\omega}_2 - u_\delta)(1+\bar{V})^2 \tag{13}$$

where the new state variables are defined as

$$\bar{V} = \frac{V - V_e}{V_e}, \quad \bar{\theta}_g = \theta_g - \theta_{g_e}, \quad \bar{\alpha} = \alpha - \alpha_e, \quad \bar{\omega}_2 = \frac{K_q}{K_M}\omega_2$$

the nondimensional time t_n and some related constants are defined as

$$\tau_s = \frac{m_3}{K_{D_e}V_e}, \quad \varepsilon_2 = -\frac{J_2}{K_q V_e^2}\frac{1}{\tau_s}, \quad t_n = t/\tau_s, \quad \varepsilon_1 = \frac{K_q}{K_M}\frac{1}{\tau_s}$$

For the new state model, the hydrodynamic forces and moment can be described as

$$D = \left(K_{D0} + K_D(\bar{\alpha} + \alpha_e)^2\right)V_e^2(1+\bar{V})^2 \tag{14}$$

$$L = (K_{L0} + K_L(\bar{\alpha} + \alpha_e))V_e^2(1+\bar{V})^2 \tag{15}$$

$$M_2 = (K_{M0} + K_M\alpha + K_q\bar{\omega}_2)V_e^2(1+\bar{V})^2 \tag{16}$$

$$F_\delta = K_{F_\delta}u_\delta V_e^2(1+\bar{V})^2 \tag{17}$$

The system can be further written in a compact form

$$\frac{d\xi}{dt_n} = f(\xi, \eta, u_\delta) \tag{18}$$

$$\mu\frac{d\eta}{dt_n} = Ag(\xi, \eta, \varepsilon, u_\delta) \tag{19}$$

where

$$\xi = \begin{bmatrix}\bar{V}\\ \bar{\theta}_g\end{bmatrix}, \quad \eta = \begin{bmatrix}\bar{\alpha}\\ \bar{\omega}_2\end{bmatrix}, \quad A = \begin{bmatrix}\frac{\mu}{\varepsilon_1} & 0\\ 0 & \frac{\mu}{\varepsilon_2}\end{bmatrix}, \quad \varepsilon = \begin{bmatrix}\varepsilon_1\\ \varepsilon_2\end{bmatrix},$$

$$f = \begin{bmatrix}f_1\\ f_2\end{bmatrix}, \quad g = \begin{bmatrix}g_1\\ g_2\end{bmatrix}, \quad \mu = \max(\varepsilon_1, \varepsilon_2)$$

where f and g are defined accordingly based on Eqs. (10)–(13).

From singular perturbation analysis [18,19], by setting $\mu = 0$, we arrive at $\bar{\omega}_2 = 0$ and $\bar{\alpha} = u_\delta$. This is the approximated solution for the fast dynamics when the system time scale μ is small enough. Plugging those two fast-mode states into the other two state equations, we will get the reduced model for the full system. Now, we further set $\bar{\alpha} = 0$ in the reduced model for design convenience, since $\bar{\alpha}$ is relatively small in value. Then, we get the approximation of the reduced model as

$$\frac{d\xi}{dt_n} = f(\xi, 0, u_\delta) \tag{20}$$

and this second-order system will be used in the controller design. The effectiveness of designing the controller based on the approximated reduced system for the original full system will be demonstrated in Sec. 3.

3 Passivity-Based Controller Design

3.1 Passivity-Based Controller for the Approximated Reduced Model. The open-loop reduced model (Eq. (20)) with $u_\delta = 0$ has an exponentially stable equilibrium point at the origin, which can be proven by Lyapunov analysis with the following positive definite Lyapunov function [13]:

$$\Phi = \frac{2}{3} - (1+\bar{V})\cos\bar{\theta}_g + \frac{1}{3}(1+\bar{V})^3 \tag{21}$$

and $(\partial\Phi/\partial\xi)f(\xi, 0, 0) \le -b_1\|\xi\|$ with $b_1 > 0$.

Now, we want to design a feedback controller to stabilize the origin of the approximated reduced model, which also provides a faster convergence speed. The approximated reduced system is linear in control

$$\frac{d\xi}{dt_n} = f(\xi, 0, 0) + g_r(\xi)u_\delta \tag{22}$$

where

$$g_{\mathrm{r}}(\xi) = \begin{bmatrix} K_{F_\delta}(1+\bar{V})^2 \sin\alpha_e / K_{D_e} \\ K_{F_\delta}(1+\bar{V})\cos\alpha_e / K_{D_e} \end{bmatrix} \tag{23}$$

For passivity-based controller design, we first need to define an output y_{r} for the approximated reduced system, to make the system passive [19]. We choose the output as

$$y_{\mathrm{r}} = \frac{\partial \Phi}{\partial \xi} g_{\mathrm{r}}(\xi) \tag{24}$$

where

$$\begin{aligned} \frac{\partial \Phi}{\partial \xi} &= \begin{bmatrix} \frac{\partial \Phi}{\partial \bar{V}} & \frac{\partial \Phi}{\partial \bar{\theta}_{\mathrm{g}}} \end{bmatrix} \\ &= \begin{bmatrix} -\cos\bar{\theta}_{\mathrm{g}} + (1+\bar{V})^2 & (1+\bar{V})\sin\bar{\theta}_{\mathrm{g}} \end{bmatrix} \end{aligned} \tag{25}$$

We check the following expression for the approximated reduced model:

$$\frac{d\Phi}{dt_{\mathrm{n}}} = \frac{\partial \Phi}{\partial \xi}\left(f(\xi,0,0) + g_{\mathrm{r}}(\xi)u_\delta\right)$$

We know that

$$\frac{\partial \Phi}{\partial \xi} f(\xi,0,0) \le 0$$

So

$$\frac{d\Phi}{dt_{\mathrm{n}}} \le u_\delta y_{\mathrm{r}}$$

Then, by the definition of a passive system, the following system

$$\begin{cases} \dfrac{d\xi}{dt_{\mathrm{n}}} = f(\xi,0,u_\delta) \\ y_{\mathrm{r}} = \dfrac{\partial \Phi}{\partial \xi} g_{\mathrm{r}}(\xi) \end{cases} \tag{26}$$

is passive. Let control u_δ for system (22) be

$$u_\delta = -\phi(y_{\mathrm{r}}) \tag{27}$$

for some function ϕ, where $y_{\mathrm{r}}u_\delta = -y_{\mathrm{r}}\phi(y_{\mathrm{r}}) \le 0$.

Now, we take Φ in Eq. (21) as the Lyapunov function for the closed-loop system (26). Then

$$\begin{aligned} \frac{d\Phi}{dt_{\mathrm{n}}} &= \frac{\partial \Phi}{\partial \xi}\left(f(\xi,0,0) + g_{\mathrm{r}}(\xi)u_\delta\right) \\ &= \frac{\partial \Phi}{\partial \xi} f(\xi,0,0) + \frac{\partial \Phi}{\partial \xi} g_{\mathrm{r}}(\xi)u_\delta \\ &\le -b_1\|\xi\| + y_{\mathrm{r}}u_\delta \end{aligned}$$

For the glider controller design, there is limitation on the magnitude of the control variable u_δ; so, in this paper, we take

$$\phi(y_{\mathrm{r}}) = \frac{1}{K_{\mathrm{c}}}\arctan(y_{\mathrm{r}}) \tag{28}$$

where K_{c} is the control parameter that is used to limit the control output magnitude. We then have

$$\frac{d\Phi}{dt_{\mathrm{n}}} \le -b_1\|\xi\| - \frac{1}{K_{\mathrm{c}}} y_{\mathrm{r}} \arctan(y_{\mathrm{r}}) \tag{29}$$

which proves the exponential stability of the origin. Furthermore, the additional negative term $-(1/K_{\mathrm{c}})y_{\mathrm{r}}\arctan(y_{\mathrm{r}})$ in the derivative of Lyapunov function provides an extra stabilization advantage. With that term, the Lyapunov function will converge to zero more quickly, which results in a faster convergence speed. That would help the glider to return to its steady gliding path with less time.

3.2 Stability Analysis for the Full Closed-Loop System. From Eqs. (23)–(25), the designed controller u_δ in Eq. (27) is dependent on the reduced model states as

$$\begin{aligned} u_\delta = \frac{1}{K_{\mathrm{c}}}\arctan\Bigg(\frac{1}{K_{D_{\mathrm{e}}}}\big(&K_{F_\delta}\cos\alpha_{\mathrm{e}}\sin\bar{\theta}_{\mathrm{g}}(1+\bar{V})^2 \\ &+ K_{F_\delta}\sin\alpha_{\mathrm{e}}(1+\bar{V})^2\left((1+\bar{V})^2 - \cos\bar{\theta}_{\mathrm{g}}\right)\big)\Bigg) \end{aligned} \tag{30}$$

If we apply the above controller to the full-order system (10)–(13), we will have the closed-loop system, expressed in the compact form as

$$\frac{dz}{dt_{\mathrm{n}}} = h(z, u_\delta(\xi)) \tag{31}$$

where the full system state vector $z = [\,\xi \quad \eta\,]^{\mathrm{T}}$.

It is challenging to establish the global stability of the origin in Eq. (31). So we focus on the local stability in this work. The linearization matrix is defined as

$$A = \left.\frac{\partial h}{\partial z}\right|_0 = \left[a_{ij}\right]_{4\times 4} \tag{32}$$

The calculated elements in the Jacobian matrix A are

$$\begin{aligned} a_{11} &= -2 - \frac{2K_{F_\delta}^2 \sin^2\alpha_{\mathrm{e}}}{K_{\mathrm{c}}K_{D_{\mathrm{e}}}^2} \\ a_{12} &= -\frac{m_0 g\cos\theta_{g_{\mathrm{e}}}}{K_{D_{\mathrm{e}}}V_{\mathrm{e}}^2} - \frac{K_{F_\delta}^2\sin\alpha_{\mathrm{e}}\cos\alpha_{\mathrm{e}}}{K_{\mathrm{c}}K_{D_{\mathrm{e}}}^2} \\ a_{13} &= -\frac{2K_D\alpha_{\mathrm{e}}}{K_{D_{\mathrm{e}}}} \\ a_{21} &= \frac{m_0 g\cos\theta_{g_{\mathrm{e}}}}{K_{D_{\mathrm{e}}}V_{\mathrm{e}}^2} + \frac{K_L\alpha_{\mathrm{e}}}{K_{D_{\mathrm{e}}}} - \frac{2K_{F_\delta}^2\sin\alpha_{\mathrm{e}}\cos\alpha_{\mathrm{e}}}{K_{\mathrm{c}}K_{D_{\mathrm{e}}}^2} \\ a_{22} &= \frac{m_0 g\sin\theta_{g_{\mathrm{e}}}}{K_{D_{\mathrm{e}}}V_{\mathrm{e}}^2} - \frac{K_{F_\delta}^2\cos^2\alpha_{\mathrm{e}}}{K_{\mathrm{c}}K_{D_{\mathrm{e}}}^2} \\ a_{23} &= K_L/K_{D_{\mathrm{e}}} \\ a_{14} &= 0, \quad a_{24} = 0, \quad a_{31} = a_{21}, \quad a_{32} = a_{22}, \quad a_{33} = a_{23} \\ a_{41} &= -\frac{1}{\varepsilon_2}\frac{2K_{F_\delta}\sin\alpha_{\mathrm{e}}}{K_{\mathrm{c}}K_{D_{\mathrm{e}}}} \\ a_{42} &= -\frac{1}{\varepsilon_2}\frac{K_{F_\delta}\cos\alpha_{\mathrm{e}}}{K_{\mathrm{c}}K_{D_{\mathrm{e}}}} \\ a_{34} &= 1/\varepsilon_1, \quad a_{43} = -1/\varepsilon_2, \quad a_{44} = -1/\varepsilon_2 \end{aligned}$$

By examining the A matrix for the Hurwitz property, we would know whether the closed-loop system with the passivity-based controller is asymptotically stable at its equilibrium. However, it is technically difficult to check this 4×4 matrix directly unless we use a numerical approach. But due to the time-scale separation property of system (Eq. (31)), there is an alternative way to check the stability, by checking two 2×2 matrices on their Hurwitz property [20].

First, we break the matrix A into four blocks using four 2×2 matrices A_{11}, A_{12}, A_{21}, and A_{22}. Here

$$A=\begin{bmatrix} A_{11} & A_{12} \\ \frac{1}{\mu}A_{21} & \frac{1}{\mu}A_{22} \end{bmatrix}$$

Following [20], instead of checking matrix A, we only need to check 2×2 matrices A_{22} and $A_{11}-A_{12}A_{22}^{-1}A_{21}$ on whether they are Hurwitz, for proving the stability of the full-order system when μ is sufficiently small. Plugging the calculated elements of linearization matrix A into those four matrices, we have

$$A_{22}=\begin{bmatrix} \mu\frac{K_L}{K_{D_e}} & \frac{\mu}{\varepsilon_1} \\ -\frac{\mu}{\varepsilon_2} & -\frac{\mu}{\varepsilon_2} \end{bmatrix},\quad A_{11}-A_{12}A_{22}^{-1}A_{21}=\begin{bmatrix} b_1 & b_2 \\ b_3 & b_4 \end{bmatrix}$$

where

$$b_1=-2-\frac{2K_{F_\delta}^2\sin^2\alpha_e}{K_cK_{D_e}^2}+\frac{4\mu^2K_{F_\delta}\alpha_e\sin\alpha_eK_D}{\varepsilon_1\varepsilon_2K_cK_{D_e}^2}$$

$$b_2=-\frac{m_0g\cos\theta_{g_e}}{K_{D_e}V_e^2}-\frac{K_{F_\delta}^2\sin\alpha_e\cos\alpha_e}{K_cK_{D_e}^2}+\frac{2\mu^2K_{F_\delta}K_D\alpha_e\cos\alpha_e}{\varepsilon_1\varepsilon_2K_cK_{D_e}^2}$$

$$b_3=\frac{m_0g\cos\theta_{g_e}}{K_{D_e}V_e^2}+\frac{K_L\alpha_e}{K_{D_e}}-\frac{2K_{F_\delta}^2\sin\alpha_e\cos\alpha_e}{K_cK_{D_e}^2}-\frac{2\mu^2K_{F_\delta}K_L\sin\alpha_e}{\varepsilon_1\varepsilon_2K_cK_{D_e}^2}$$

$$b_4=\frac{m_0g\sin\theta_{g_e}}{K_{D_e}V_e^2}-\frac{K_{F_\delta}^2\cos^2\alpha_e}{K_cK_{D_e}^2}-\frac{\mu K_{F_\delta}K_L\cos\alpha_e}{\varepsilon_1K_cK_{D_e}^2}$$

For matrix A_{22}, the characteristic equation is

$$\lambda^2+k_1\lambda+k_0=0$$

where

$$k_1=\frac{\mu}{\varepsilon_2}-\mu\frac{K_L}{K_{D_e}},\quad k_0=\frac{\mu^2}{\varepsilon_1\varepsilon_2}-\mu\frac{K_L\mu}{K_{D_e}\varepsilon_2}$$

Because $\mu\sim O(\varepsilon_i)$, i.e., μ is in the same order of the time scale ε_i, and they are both sufficiently small, it can be shown easily that the coefficients k_1 and k_0 are both positive, which means A_{22} is Hurwitz.

Now for matrix $A_{11}-A_{12}A_{22}^{-1}A_{21}$, let the coefficients of the characteristic equation be l_1 and l_0, defined similar to k_1 and k_0. It is easy to get

$$l_1=-(b_1+b_4),\quad l_0=b_1b_4-b_2b_3 \tag{33}$$

Here, we exploit information about the underwater glider system and set a range for those parameters. From the underwater glider application perspective, we have

$$\sin\alpha_e\approx\alpha_e,\quad \cos(\alpha_e)\approx 1,\quad 0\le K_{F_\delta}\sim O(10),\quad V_e\le 1,$$
$$K_{D_e}\sim O(10),\quad K_{u_\delta}\sim O(1),\quad K_{L_e}\sim O(10),$$
$$K_L\sim O(100),\quad K_D\sim O(100),\quad 0.25\le|\theta_{g_e}|\le 0.75$$

where metric units are applied to all above parameter values. Besides, we bound the control parameter K_c in an open set (1, 10) to restrain the magnitude of the control u_δ from 9 deg to 90 deg, which is consistent with the application constraints. Then, we find that for each element in the 2×2 matrix $A_{11}-A_{12}A_{22}^{-1}A_{21}$, there is a dominant term, which determines the sign of that element, with all other minor terms only influencing the value. We express the approximation using the dominant terms for the matrix elements

$$b_1\approx -2,\quad b_2\approx -\frac{m_0g\cos\theta_{g_e}}{K_{D_e}V_e^2},$$
$$b_3\approx\frac{m_0g\cos\theta_{g_e}}{K_{D_e}V_e^2},\quad b_4\approx\frac{m_0g\sin\theta_{g_e}}{K_{D_e}V_e^2}$$

Since m_0 and θ_{g_e} are always opposite in sign, $b_4<0$. We also notice that b_2 and b_3 are opposite in sign. So, from Eq. (33), we have $l_1>0$ and $l_0>0$. With all characteristic equation coefficients positive, the matrix $A_{11}-A_{12}A_{22}^{-1}A_{21}$ is Hurwitz.

From the above analysis, we have shown that the original 4×4 linearization matrix A is Hurwitz for sufficiently small μ, which proves that the passivity-based controller derived from the approximated reduced model also stabilizes the full-order system. Furthermore, by the fact that the controller is designed based on the approximated reduce system through passivity analysis, we conjecture that this controller will be similarly effective for the full system as it does for the approximated reduced system. In particular, we anticipate that the controller will provide a faster convergence speed than the open-loop controller $u_\delta=0$, due to the additional negative term it introduced into Eq. (29).

3.3 Simulation Results. We apply the passivity-based controller to the full dynamics model, and use MATLAB SIMULINK to simulate the controller performance. The glider parameters we used are: $m=10$ kg, $J_2=0.08$ kg/m^2, $K_{L0}=0$ kg/m, $K_L=303.6$ kg/m, $K_{D0}=3.15$ kg/m, $K_D=282.8$ kg/m, $K_q=-0.8$ kg/s, $K_{M0}=0.39$ kg, $K_M=-14.7$ kg, $\delta=29.5$, and $m_0=0.05$ kg. The equilibrium point is $V_e=0.24$ m/s, $\theta_{g_e}=-22.5$ deg, $\alpha_e=1.52$ deg, and $\omega_{2e}=0$ rad/s. The system parameters are chosen based on the lab-developed prototype, named "Grace." The hydrodynamic coefficients are obtained through computational fluid dynamics (CFD)-based water tunnel simulation [16,21]. Suppose that we have a current disturbance that makes the glider deviate off its steady gliding path. From that point, we want the glider to return to its equilibrium gliding profile. The initial states are given as $V_0=0.2$ m/s, $\theta_{g_0}=-35$ deg, $\alpha_0=1$ deg, and $\omega_{20}=0$ rad/s. In simulation, we also consider the dynamics of the actuator for moving the control surface, approximated by a first-order system with a time constant of 10 ms. The simulation time is 60 s.

Figure 2 shows that the passivity-based controller designed for the reduced model works for the original full-order system, not only stabilizing the steady gliding equilibrium but also speeding up the convergence process as we expected from the analysis. Figures 3–4 show the influences of the control parameter K_c on the control output and the glide angle transients. It can be seen that with a smaller K_c, the system converges faster but requires

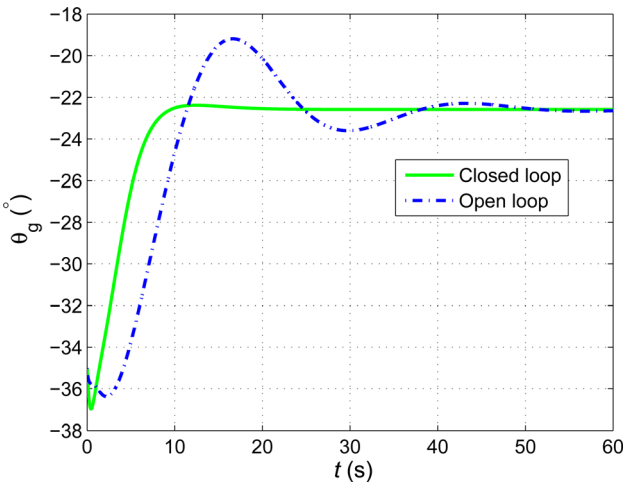

Fig. 2 Simulation results on the trajectories of the gliding angle θ_g for the open-loop $u_\delta=0$ and closed-loop ($K_c=2$) cases, respectively

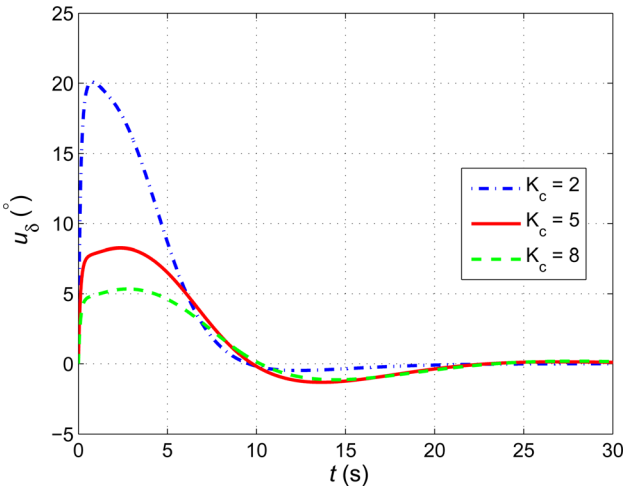

Fig. 3 The trajectory of control u_δ for the closed-loop simulation with different values for K_c

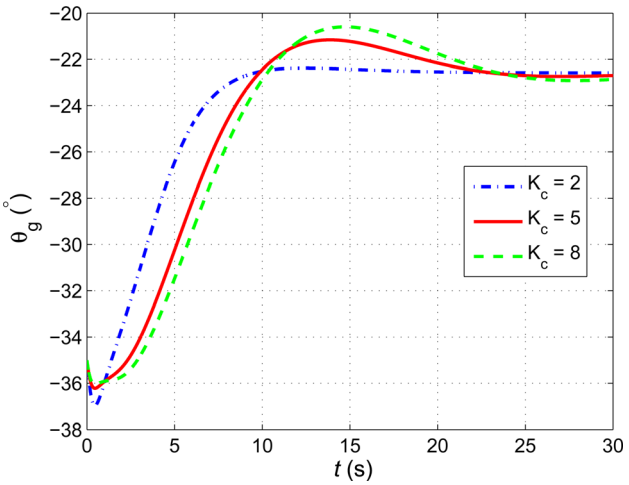

Fig. 4 The trajectory of gliding angle θ_g for the closed-loop simulation with different values for K_c

larger initial control effort. With the arctangent function in Eq. (28), the tunable parameter K_c makes it easy to balance between the control effort and the convergence speed.

4 Observer Design

In this section, we propose a nonlinear model-based observer to estimate the velocity V and the gliding angle θ_g (see Eq. (30)), using only the pitch angle which can be measured from onboard sensors. The local stability of the observer is analyzed with a constructed Lyapunov function.

A nonlinear observer is proposed in order to estimate system states with a relatively large convergence region. The observer gain structure is selected to be linear, to enable efficient computation and onboard implementation in experiments. The gain is obtained by solving the Riccati equation as in the Extended Kalman filter, in order to take the robustness to the measurement noise into the design consideration. The nonlinear observer can be expressed as

$$\dot{\hat{\boldsymbol{x}}} = f(\hat{\boldsymbol{x}}, u_\delta) + H_o(\theta - \hat{\theta}) \tag{34}$$

$$\hat{\theta} = h(\hat{\boldsymbol{x}}) \tag{35}$$

Here, $\hat{\boldsymbol{x}} = [\hat{V} \quad \hat{\theta}_g \quad \hat{\alpha} \quad \hat{\omega}_2]^T$ is the estimated system state, $f(\hat{\boldsymbol{x}}, u_\delta)$ is the observer dynamics, as described in Eqs. (6)–(9), $h(\hat{\boldsymbol{x}}) = \hat{\theta}_g + \hat{\alpha}$ is the output function, and H_o is the observer gain.

Let Q be a 4×4 symmetric positive definite matrix, which denotes the process noise covariance for the state dynamics. Let R be a constant, representing the measurement noise variance. Let P be the solution of the Riccati equation

$$A_o P + P A_o^T + Q - P C_o^T R^{-1} C_o P = 0 \tag{36}$$

where A_o and C_o are the linearization matrix of the system

$$A_o = \begin{bmatrix} -\frac{1}{m_1}\frac{\partial D}{\partial V} & -\frac{m_0 g \cos\theta_g}{m_1} & -\frac{1}{m_1}\frac{\partial D}{\partial \alpha} & 0 \\ \frac{1}{m_1 V}\frac{\partial L}{\partial V} & \frac{m_0 g \sin\theta_g}{m_1 V} & \frac{1}{m_1 V}\frac{\partial L}{\partial \alpha} & 0 \\ -\frac{1}{m_1 V}\frac{\partial L}{\partial V} & -\frac{m_0 g \sin\theta_g}{m_1 V} & -\frac{1}{m_1 V}\frac{\partial L}{\partial \alpha} & 1 \\ \frac{2V(K_{M0} + K_M \alpha)}{J_2} & 0 & \frac{K_M V^2}{J_2} & \frac{K_{q2} V^2}{J_2} \end{bmatrix}_e$$

$$C_o = [0 \quad 1 \quad 1 \quad 0]$$

Here, $[\cdot]_e$ means that matrix elements are evaluated at the equilibrium point.

$$\frac{\partial L}{\partial \alpha} = K_L V^2, \quad \frac{\partial L}{\partial V} = 2V(K_{L0} + K_L \alpha),$$
$$\frac{\partial D}{\partial \alpha} = 2K_D V^2 \alpha, \quad \frac{\partial D}{\partial V} = 2V(K_{D0} + K_D \alpha^2)$$

The existence of a positive definite matrix P is guaranteed by the observability of (A_o, C_o). If P exists, the observer gain H_o can be designed as

$$H_o = P C_o^T R^{-1} \tag{37}$$

By tuning the value of R, we can adjust the robustness of the observer to different levels of measurement noise.

The stability of the designed nonlinear observer is analyzed below. We first define the dynamics system states as $\boldsymbol{x} = [V \quad \theta_g \quad \alpha \quad \omega_2]^T$. Then, the system dynamics can be expressed as

$$\dot{\boldsymbol{x}} = f(\boldsymbol{x}, u_\delta) \tag{38}$$

$$\theta = h(\boldsymbol{x}) \tag{39}$$

Define the state estimation error as $\tilde{\boldsymbol{x}} = \boldsymbol{x} - \hat{\boldsymbol{x}}$, and then from Eqs. (34) (35), (38), and (39) we have the estimation error dynamics

$$\dot{\tilde{\boldsymbol{x}}} = f(\boldsymbol{x}, u_\delta) - f(\hat{\boldsymbol{x}}, u_\delta) - H_o(h(\boldsymbol{x}) - h(\hat{\boldsymbol{x}})) \tag{40}$$

Taylor series of functions f and h are taken at the equilibrium point, and we have

$$\dot{\tilde{\boldsymbol{x}}} = (A_o - H_o C_o)\tilde{\boldsymbol{x}} + \eta(\tilde{\boldsymbol{x}}, t) \tag{41}$$

Here, $\eta(\tilde{\boldsymbol{x}}, t)$ represents the sum of Taylor series terms that contain second-order and higher-order $\tilde{\boldsymbol{x}}$. Furthermore, $\eta(0, t) = 0$. There exist positive constants c_0 and k_1 such that when estimation error $|\tilde{\boldsymbol{x}}| < c_0$, we have

$$\|\eta(\tilde{\boldsymbol{x}}, t)\| \le k_1 \|\tilde{\boldsymbol{x}}\|^2 \tag{42}$$

We define a Lyapunov function $V(\tilde{x})$ for the system (Eq. (41))

$$V(\tilde{x}) = \tilde{x}^T P^{-1} \tilde{x} \tag{43}$$

We take the time derivative of $V(\tilde{x})$

$$\dot{V}(\tilde{x}) = \tilde{x}^T P^{-1} \dot{\tilde{x}} + \dot{\tilde{x}}^T P^{-1} \tilde{x} \tag{44}$$

From Eqs. (36), (37), (41), and (44), we have

$$\dot{V}(\tilde{x}) = -\tilde{x}^T (C_0^T R^{-1} C_0 + P^{-1} Q P^{-1}) \tilde{x} + 2\tilde{x}^T P^{-1} \eta(\tilde{x}, t) \tag{45}$$

Here $(C_0^T R^{-1} C_0 + P^{-1} Q P^{-1}) \geq \sigma_{\min} \mathbf{1}_{4\times 4}$ is positive definite, and $\sigma_{\min}$ is a finite scaler. From Eq. (42), the time derivative of Lyapunov function is bounded

$$\dot{V}(\tilde{x}) \leq -c_1 \|\tilde{x}\|^2 + c_2 \|\tilde{x}\|^3 \tag{46}$$

Here, c_1 and c_2 are positive scalar coefficients that depend on the noise signals and the system matrices. The coefficients can be selected as

$$c_1 = \sigma_{\min}, \quad c_2 = 2k_1 \|P^{-1}\| \tag{47}$$

It can be easily shown from Eq. (46) that the state estimation error $\tilde{x}$ dynamics is locally exponentially stable. Furthermore, the local exponential stability of the full closed-loop system can be verified by the separation principle [19] with the proven local exponential stability property of the passivity-based controller and the nonlinear observer.

We also consider the influence of the system noise and measurement noise on the observer stability. The noise-corrupted system dynamics can be expressed as

$$\dot{x} = f(x, u_\delta) + \nu_1 \tag{48}$$

$$\theta = h(x) + \nu_2 \tag{49}$$

where ν_1 and ν_2 represent the process noise and measurement noise, respectively. The state estimation error dynamics for such a system is

$$\dot{\tilde{x}} = f(x, u_\delta) - f(\hat{x}, u_\delta) - H_o(h(x) - h(\hat{x})) + \nu_1 - H_o \nu_2 \tag{50}$$

Taylor series of functions f and h are taken at the equilibrium point, and we have

$$\dot{\tilde{x}} = (A_o - H_o C_o)\tilde{x} + \eta(\tilde{x}, t) + \xi(t) \tag{51}$$

Here, $\xi(t) = \nu_1 - H_o \nu_2$. Assuming that the noise signals ν_1 and ν_2 are bounded, there exist constant k_1 and k_2 such that

$$\|\eta(\tilde{x}, t)\| \leq k_1 \|\tilde{x}\|^2, \quad \|\xi(t)\| \leq k_2 \tag{52}$$

We take the same Lyapunov function $V(\tilde{x})$ for the system (Eq. (51))

$$V(\tilde{x}) = \tilde{x}^T P^{-1} \tilde{x} \tag{53}$$

From Eqs. (36), (37), (44), and (51), the time derivative of $V(\tilde{x})$ is

$$\dot{V}(\tilde{x}) = -\tilde{x}^T (C_0^T R^{-1} C_0 + P^{-1} Q P^{-1}) \tilde{x} + 2\tilde{x}^T P^{-1} (\eta(\tilde{x}, t) + \xi(t)) \tag{54}$$

Because of the boundedness properties of the noise signal, the time derivative of Lyapunov function is bounded

$$\dot{V}(\tilde{x}) \leq -c_1 \|\tilde{x}\|^2 + c_2 \|\tilde{x}\|^3 + c_3 \|\tilde{x}\| \tag{55}$$

Here, c_1, c_2, and c_3 are positive scalar coefficients that depend on the noise signals and the system matrices. The coefficients can be selected as

$$c_1 = \sigma_{\min}, \quad c_2 = 2k_1 \|P^{-1}\|, \quad c_3 = 2k_2 \|P^{-1}\| \tag{56}$$

It can be shown from Eq. (55) that the state estimation error will be bounded

$$|\tilde{x}| \leq \frac{c_1}{2c_2} \quad \text{when} \quad 4c_2 c_3 - c_1^2 \leq 0 \quad \text{and} \quad \frac{c_1}{2c_2} < c_0 \tag{57}$$

The condition inequalities in Eq. (57) can be checked for a given system with known system matrices and the noise signal characteristics. We speculate that the stabilization output of the full closed-loop system will also be bounded around the nominal value, based on the boundedness of the state estimation error and the exponential stability of the designed passivity-based controller.

Simulation is carried out to examine the performance of the designed observer. The closed-loop system with the passivity-based controller for stabilization is simulated with full state feedback. The observer runs in parallel with the closed-loop dynamics with the measured pitch angle as the observer input. In simulation, measurement noise $\upsilon(t)$, added to the system output $\theta(t)$, is modeled as a Gaussian random process with zero-mean, $E\{\upsilon\} = 0$, and variance R, $E\{\upsilon(t)\upsilon(\tau)\} = R\delta(t-\tau)$. Figure 5 shows the noise-corrupted system output, the measured pitch angle with the variance of measurement noise $R = 0.1$. Figure 6 shows both the real and estimated gliding angle trajectories. Gliding angle θ_g is used here to evaluate the effectiveness of state estimation because it is the signature variable in the sagittal-plane glide motion. Control parameter $K_c = 2$ is used. The simulation results show that the proposed observer is able to estimate the system states with good robustness to the measurement noise.

5 Experimental Results

In order to test the effectiveness of the proposed passivity-based controller (Sec. 3.1) and the nonlinear observer (Sec. 4), we conduct both open-loop and closed-loop experiments using a gliding robotic fish. A gliding robotic fish is a new type of underwater robots that features both energy efficiency of underwater gliders and high maneuverability of robotic fish [22,16]. The robot

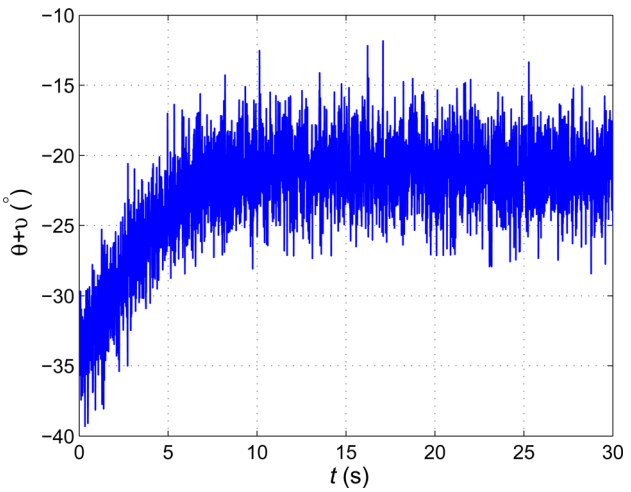

Fig. 5 Simulated trajectory of the measured pitch angle, which is corrupted with noise. The measurement noise is modeled as Gaussian random process with $R = 0.1$.

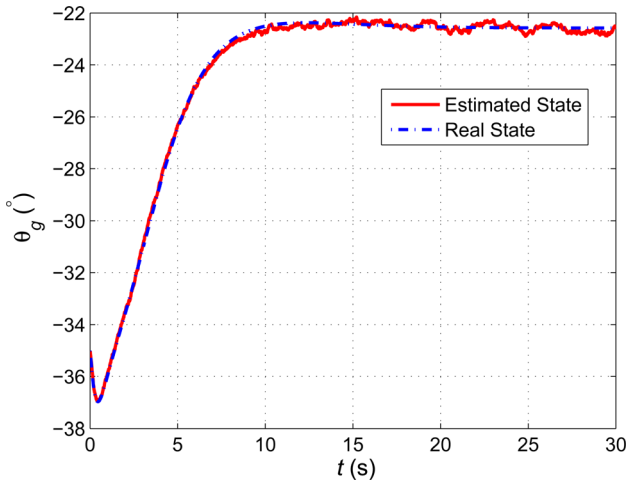

Fig. 6 Simulation results: the trajectories of the gliding angle θ_g of the real state and nonlinear observer estimation with measurement noise.

used in this work, named Grace, has three actuation systems for locomotion, including the buoyancy system, the mass distribution system, and the actively controlled tail fin system. In the buoyancy system, water is pumped in and out of the robot's body to change the net buoyancy. When the robot is heavier than the water it displaces (negatively buoyant), the robot will descend; and when it is lighter than the water it displaces (positively buoyant), the robot will ascend. The tail fin system in Grace is driven by a servomotor (Hitec Servo HS-7980TH) through a chain transmission. In experiments, the tail is adjusted up or down like a whale fluke to modulate the glide motion. A microcontroller (dsPIC 30F6014A) in the robot runs the glide control program and provides storage memory for the measurement data. Grace is also equipped with the IMUs including gyros (ST LPY503AL), accelerometers, and a digital compass (ST LSM303DLMTR), which are used to measure the robot's attitude.

5.1 Filter Design. The IMU sensor output is corrupted with a high-frequency noise. The system output, namely, the pitch angle, is computed from the accelerometer sensor output. In this work, in order to smooth the measured pitch angle, a second-order Butterworth digital filter is adopted. The discrete-time transfer function of the filter can be expressed as

$$H(z) = \frac{a_0 + a_1 z^{-1} + a_2 z^{-2}}{1 + b_1 z^{-1} + b_2 z^{-2}} \tag{58}$$

where a_0, a_1, a_2, b_1, and b_2 are filter coefficients.

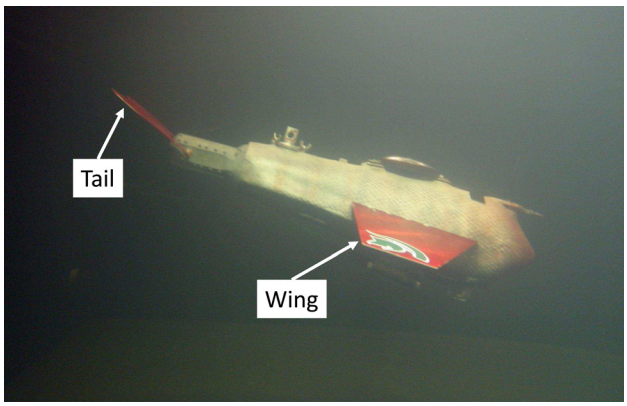

Fig. 7 A snapshot of the open-loop experiment with fixed tail angle using gliding robotic fish Grace in the lab tank

Let f_r denote the ratio between the sampling frequency f_s and the cutoff frequency f_c

$$f_r = \frac{f_s}{f_c} \tag{59}$$

For the Butterworth filter, the above coefficients can be determined as the follows:

$$a_0 = a_2 = \frac{\omega_c'^2}{c}$$
$$a_1 = 2a_0$$
$$b_1 = \frac{2(\omega_c'^2 - 1)}{c}$$
$$b_2 = \frac{1 - 2\cos(\pi/4)\omega_c' + \omega_c'^2}{c}$$

where $\omega_c' = \tan(\pi/f_r)$, and $c = 1 + 2\cos(\pi/4)\omega_c' + \omega_c'^2$.

In this work, the sampling frequency is 50 Hz, and the cutoff frequency is designed to be 10 Hz. The low-pass Butterworth filter

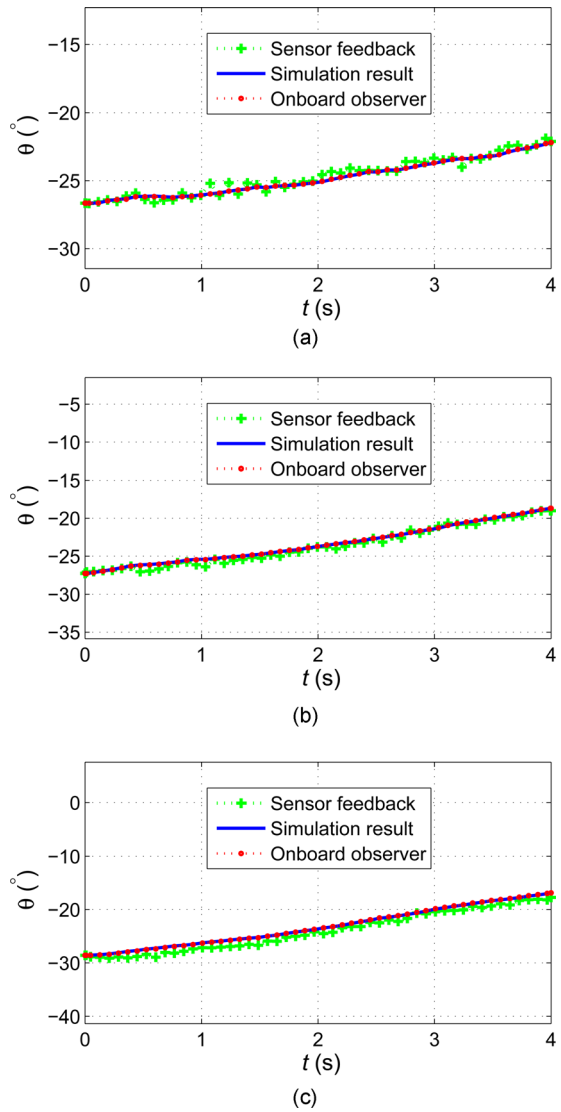

Fig. 8 The trajectories of pitch angle of the on-board sensor reading, observer estimation, and computer-based simulation result, in the open-loop experiments using gliding robotic fish Grace. (*a*) $\delta = 15$ deg; (*b*) $\delta = 30$ deg; and (*c*) $\delta = 45$ deg.

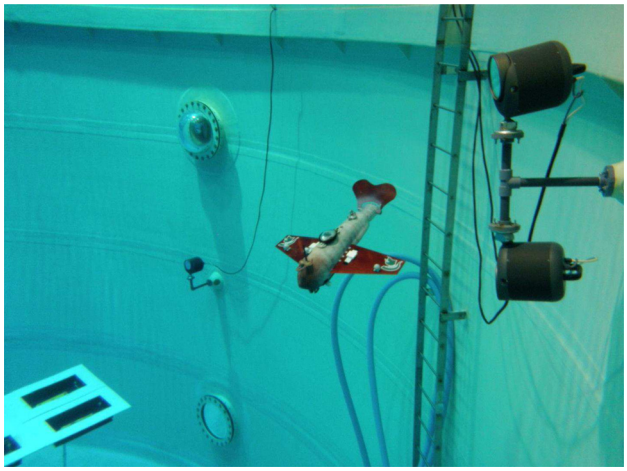

Fig. 9 A snapshot of stabilization experiment using gliding robotic fish Grace in NBRF, University of Maryland

for the pitch angle can be described using the following recursive difference equation:

$$\theta(n) = a_0\theta_s(n) + a_1\theta_s(n-1) + a_2\theta_s(n-2) - b_1\theta(n-1) - b_2\theta(n-2) \quad (60)$$

where $\theta(n)$ and $\theta_s(n)$ are the Butterworth filter's output and input (pitch angle) at the nth step, respectively. In this work, $a_0 = a_2 = 0.20644$, $a_1 = 0.41289$, $b_1 = -0.3702$, and $b_2 = 0.19597$.

5.2 Open-Loop Experiments. Open-loop experiments are first conducted in a large indoor tank, which measures 5 m long, 3.3 m wide, and 1.3 m deep, using the gliding robotic fish prototype named Grace (Fig. 7). The robot is first released from the water surface with a fixed tail angle δ, and then water is pumped into the robot's body until the net buoyancy m_0 reaches 50 g. Two seconds after the gliding down motion is initiated, the observer is initialized in the microcontroller. During the following period, the robot records the pitch angle readings from both onboard sensors and the observer. The readings are further compared together with the pure computer-based MATLAB simulation result, which is obtained by running the same observer dynamics continuously in MATLAB based on the sensor output history recorded onboard. Figure 8 shows the experimental results on the pitch angle θ for different fixed tail angles $\delta = 15$ deg, 30 deg, and 45 deg, where the measured pitch angle is compared with the values derived from the state estimate with Eq. (35). First, we can observe that the computer-based MATLAB simulation of the nonlinear observer produces estimate trajectories almost identical to those from the onboard observer, confirming that the microcontroller is able to execute the observer with little loss in accuracy. Second, the match between the observer estimation and sensor output further validates the design of the nonlinear observer.

5.3 Closed-Loop Experiments. In this subsection, experimental results on sagittal-plane stabilization using the passivity-based controller are presented to verify the effectiveness of both the proposed nonlinear controller and the nonlinear observer. Experiments are conducted in the Neutral Buoyancy Research Facility (NBRF) at the University of Maryland, College Park, which is a water tank measuring 15 m across and 7.5 m deep.

In the experiments, the robot is released from the water surface with a net buoyancy $m_0 = 50$ g. The tail angle δ is initially set to 60 deg. Then, the robot enters gliding down motion. When the robot reaches a preset depth of 1 m, the tail flaps to $\delta = 0$ deg to provide an initial perturbation for the stabilization process. Then, the designed passivity-based controller (Eq. (30)) kicks in to stabilize the system, with the state estimation using the nonlinear observer (Fig. 9). A Qualysis underwater motion capture system, which consists of 12 underwater cameras and motion tracking software, is used to record the whole stabilization process and analyze the motion afterwards (Fig. 10).

Figure 11 shows the experimental results on three types of pitch angle trajectories including onboard sensor measurements, onboard observer estimation, and motion capture system output, together with the onboard gliding angle estimation, when no feedback control exists, with tail angle trajectory designed as in Fig. 12. Figures 13–16 show the experimental results for passivity-based stabilization for two different values of the controller gain. From the experimental results, we observe a good

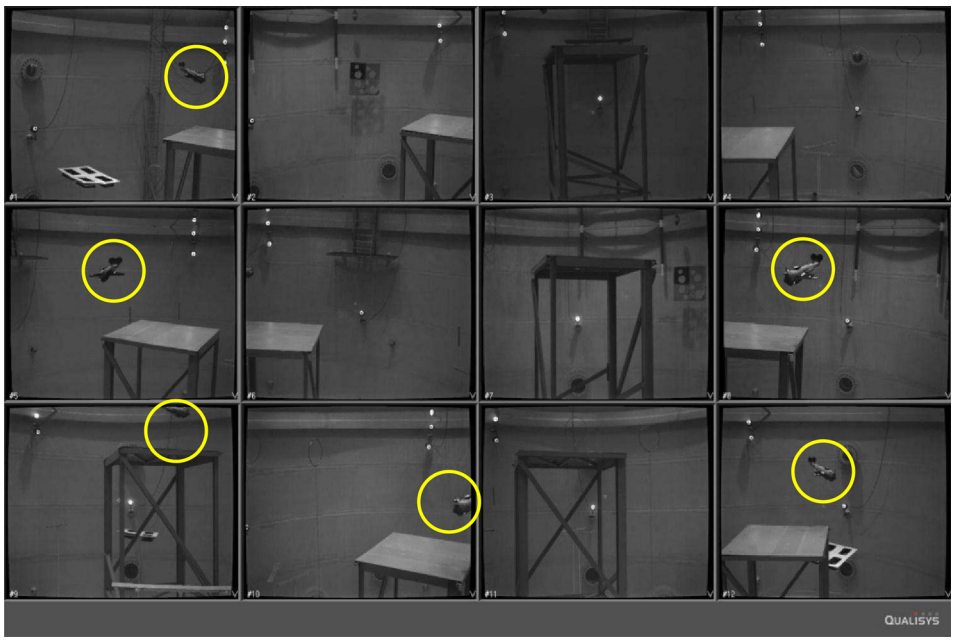

Fig. 10 A snapshot of stabilization experiment in the view of the 12 underwater cameras of the qualysis motion capture system in NBRF, University of Maryland

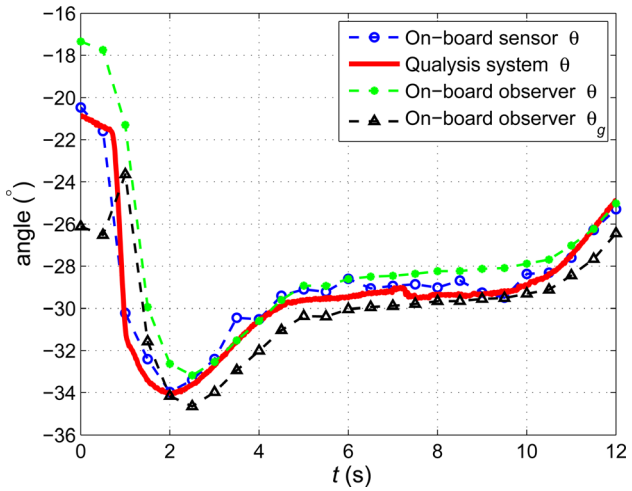

Fig. 11 The trajectories of pitch angle and gliding angle in the experiment of gliding stabilization without feedback control

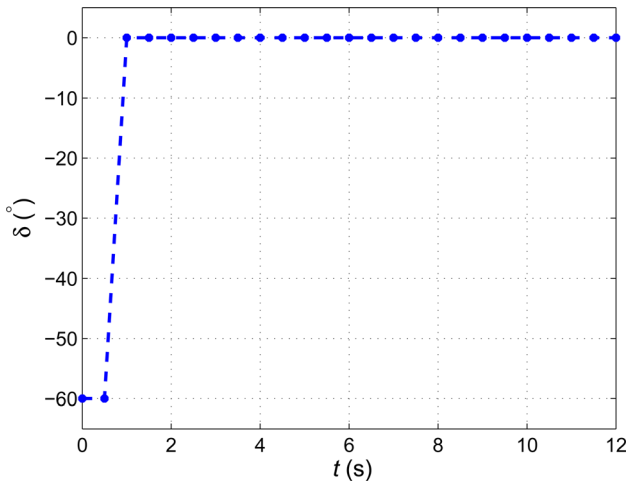

Fig. 12 The trajectory of predefined tail angle in the experiment of gliding stabilization without feedback control

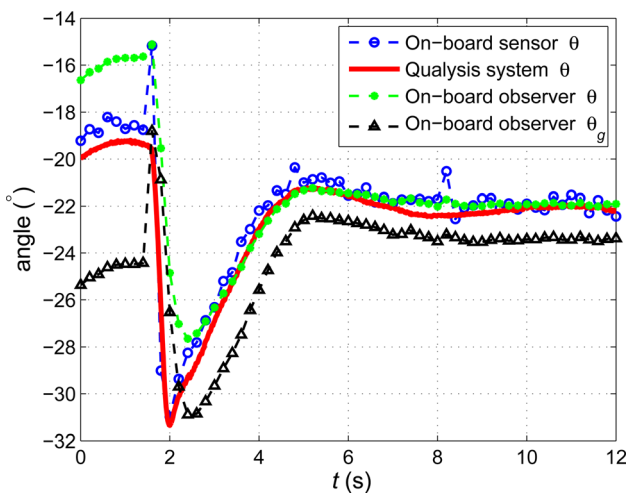

Fig. 13 The trajectories of pitch angle and gliding angle in the passivity-based stabilization experiment with $K_c = 3$

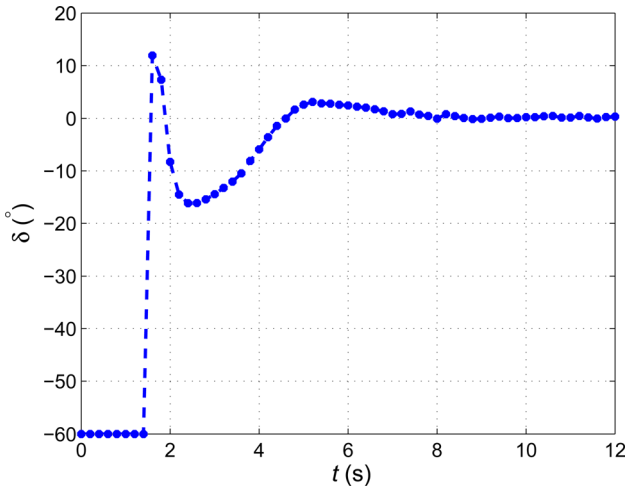

Fig. 14 The trajectory of tail angle in the passivity-based stabilization experiment with $K_c = 3$

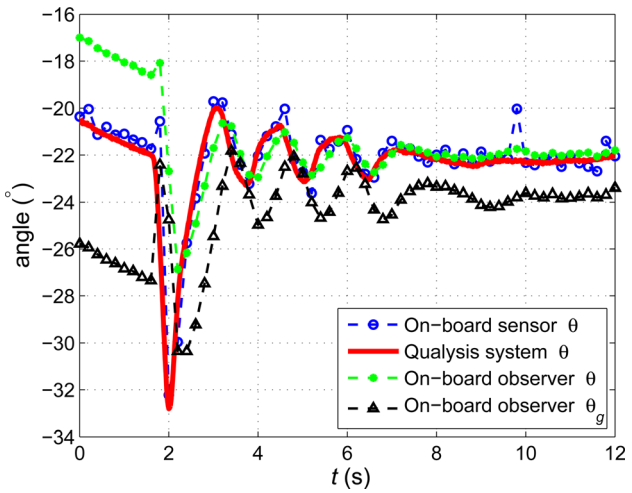

Fig. 15 The trajectories of pitch angle and gliding angle in the passivity-based stabilization experiment with $K_c = 1$

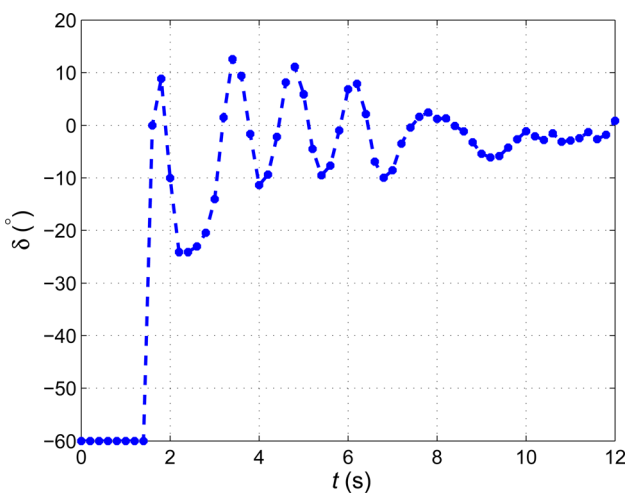

Fig. 16 The trajectory of tail angle in the passivity-based stabilization experiment with $K_c = 1$

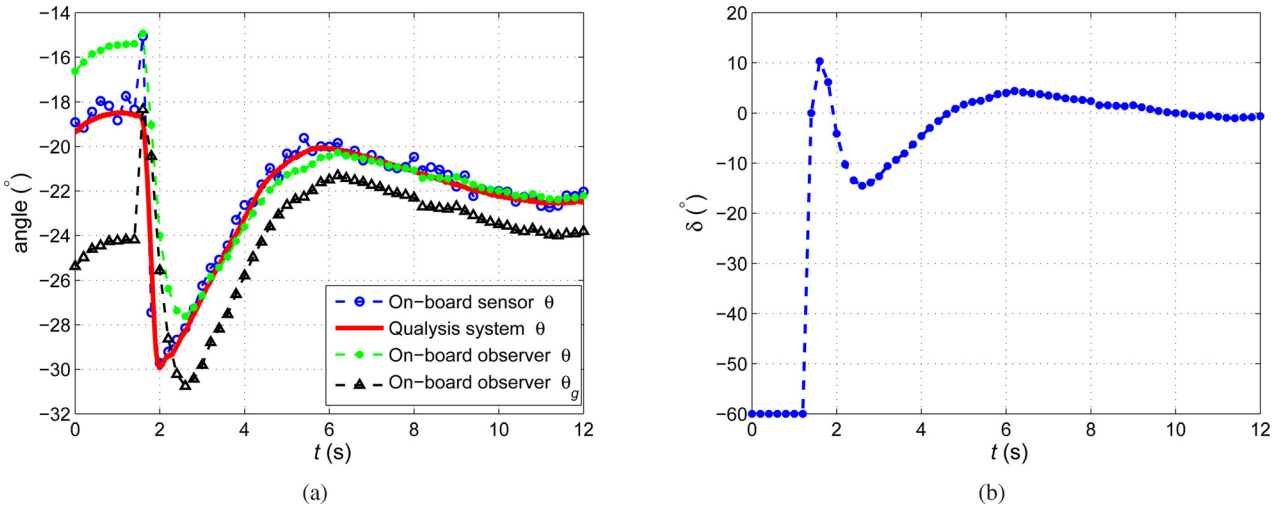

(a) (b)

Fig. 17 The trajectories in the comparative stabilization experiments with a proportional controller with $K_P = 2$. (*a*) pitch angle and gliding angle and (*b*) tail angle.

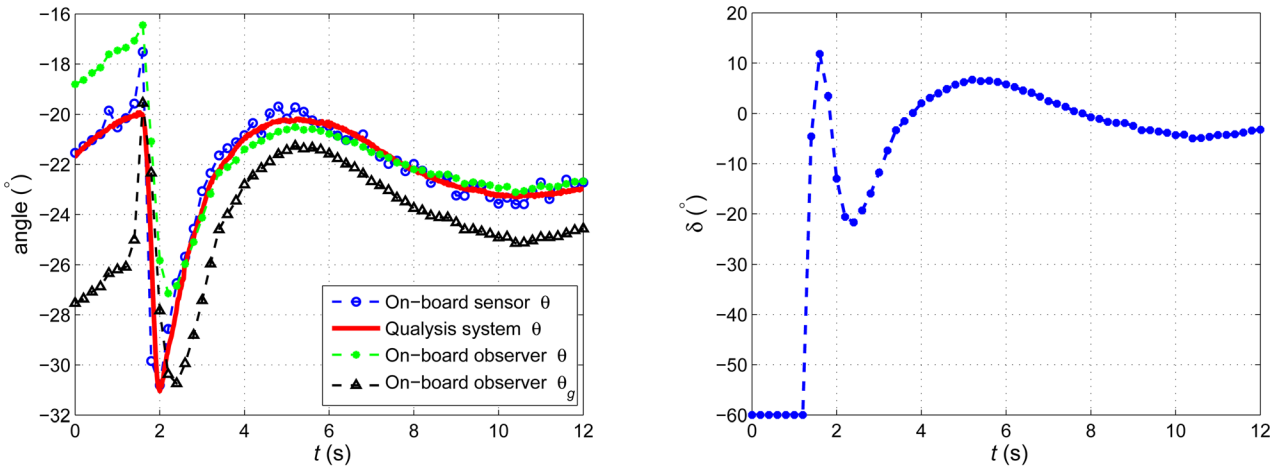

(a) (b)

Fig. 18 The trajectories in the comparative stabilization experiments with a proportional controller with $K_P = 3$. (*a*) pitch angle and gliding angle and (*b*) tail angle.

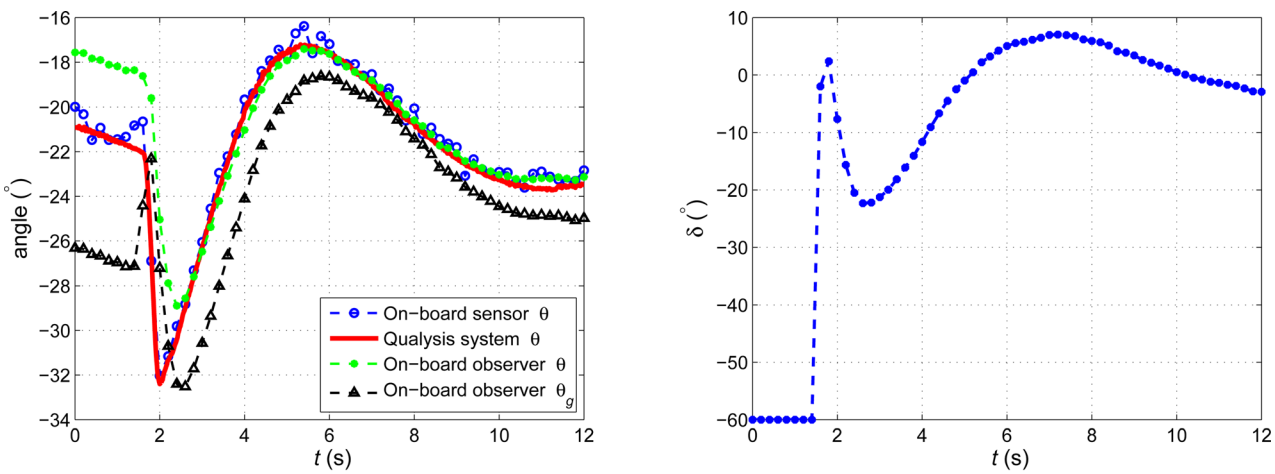

(a) (b)

Fig. 19 The trajectories in the comparative stabilization experiments with a PI controller with $K_P = 2$ and $K_I = 1$. (*a*) pitch angle and gliding angle and (*b*) tail angle

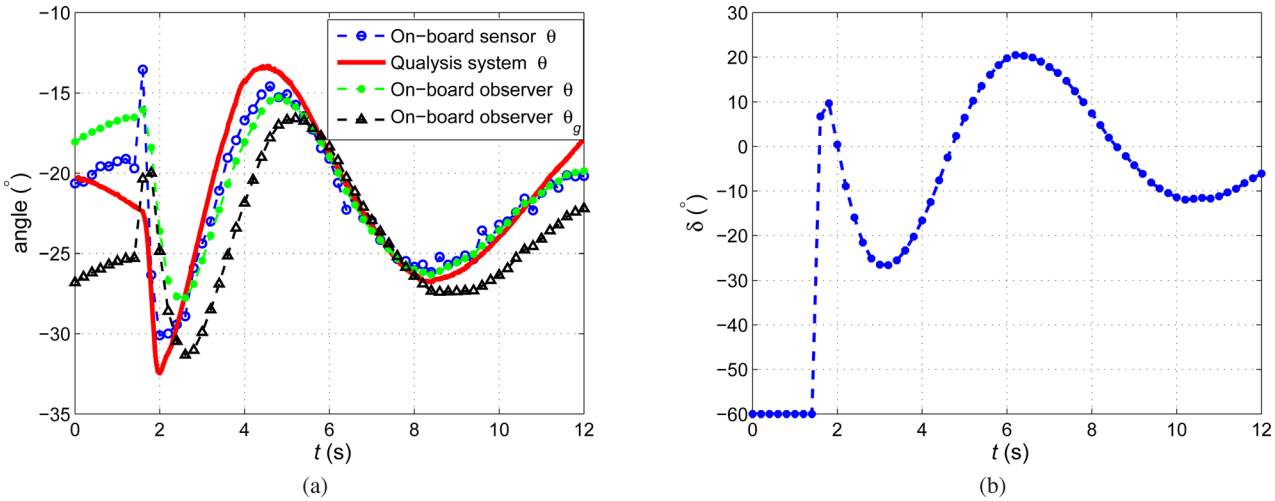

Fig. 20 The trajectories in the comparative stabilization experiments with a PI controller with $K_P = 2$ and $K_I = 3$. (*a*) pitch angle and gliding angle and (*b*) tail angle.

match among the pitch angle estimation, the on-board sensor reading, and the motion capture system output. The results further verify the proposed nonlinear observer design. Besides, the gliding angle converges to the equilibrium point around −23.5 deg. The results confirm that the passivity-based controller effectively stabilizes the sagittal-plane glide motion and speeds up the convergence process, comparing with the glide angle trajectory in the open-loop case (Fig. 11). It also shows that with a smaller controller gain K_c, the arising time of the pitch angle is shorter (1 s in Fig. 15 versus 2 s in Fig. 13) and the control output magnitude is larger (25 deg in Fig. 16 versus 15 deg in Fig. 14), which is consistent with and complementary to the simulation findings in Sec. 3.3. This provides insight into the control parameter design in order to balance between convergence time and control efforts.

In experiments, we also implemented proportional controller and PI controller for glide stabilization for the purpose of comparison. Experimental results using a proportional controller and a PI controller are shown in Figs. 17, 18, 19, and 20, respectively. We varied the controller parameters, the proportional gain K_P and the integral gain K_I in order to obtain a better performance. We find that with a larger K_P and K_I, the arising time of the gliding angle trajectory is reduced, however, with the cost of larger overshoot and oscillation amplitude, which shows similar tradeoff in tuning the passivity-based controller gain. Furthermore, in the comparison of the experimental results between using P/PI control and using passivity-based control, the differences in arising time, percent overshoot, and oscillation time show that the passivity-based controller has an overall better performance than the P/PI controller, especially in terms of the balance between convergence speed and control effort.

6 Conclusion and Future Work

In this paper, we proposed a new systematic stabilization method for underwater gliders. The controller design was based on passivity analysis, for the approximated reduced model, which was derived from the full-order system through singular perturbation analysis. The local exponential stability was shown for the full closed-loop system by checking the Hurwitz property of the Jacobian matrix. With the additional negative term appearing in the time derivative of the Lyapunov function, we conjectured that this control scheme provides a faster convergence performance. The proposed nonlinear observer, which is proved to converge in state estimation errors, presented satisfying performance, especially in terms of robustness against the measurement noise. Both simulation and experimental results were presented to further verify the design of the full closed-loop system. The proposed stabilization method shows promise for the stabilization of underwater gliders because of its faster convergence speed, simplicity in implementation (using the state of the reduced system only), and ease in tuning the controller, compared with the traditional P/PI controllers.

The proposed controller will be especially useful in the task of shallow-water sampling, which is a main application of our lab-developed prototype Grace. In addition, since it is difficult to localize an underwater glider when it is under water, fast convergence to the steady glide path is instrumental for correctly relating the measurements to spatial locations, because the actual path taken by the glider is closer to the planned path. While feedback control, in general, and the proposed passivity-based control, in particular, will seemingly consume more energy than an open-loop controller due to the actuation needed for path correction, they will prevent large deviation from the planned path. Such deviations would often occur under open-loop control due to typical environmental disturbances, and they ultimately take more energy to correct.

For future work, we will examine the extension of the proposed passivity-based controller to several other problems of interest for underwater gliders, including tail-actuated yaw stabilization [16] and trajectory tracking in the three-dimensional underwater space with tail-enabled spirals [23].

Acknowledgment

The authors would like to thank Dr. Hassan Khalil for his insightful comments and suggestions on the passivity-based controller design, and thank Dr. Derek A. Paley and Nitin Sydney at the University of Maryland for their help in conducting experiments in the Neutral Buoyancy Research Facility.

This work was supported in part by NSF (IIS 0916720, IIS 1319602, CCF 1331852, IIP 1343413).

References

[1] Rudnick, D. L., Davis, R. E., Eriksen, C. C., Fratantoni, D. M., and Perry, M. J., 2004, "Underwater Gliders for Ocean Research," Mar. Technol. Soc. J., **38**(2), pp. 73–84.

[2] Eriksen, C. C., Osse, T. J., Light, R., Wen, R. D., Lehmann, T. W., Sabin, P. L., Ballard, J. W., and Chiodi, A. M., 2001, "Seaglider: A Long-Range Autonomous Underwater Vehicle for Oceanographic Research," IEEE J. Oceanic Eng., **26**(4), pp. 424–436.

[3] Sherman, J., Davis, R. E., Owens, W. B., and Valdes, J., 2001, "The Autonomous Underwater Glider'Spray," IEEE J. Oceanic Eng., **26**(4), pp. 437–446.

[4] Webb, D. C., Simonetti, P. J., and Jones, C. P., 2001, "Slocum: An Underwater Glider Propelled by Environmental Energy," IEEE J. Oceanic Eng., **26**(4), pp. 447–452.
[5] Graver, J. G., 2005, "Underwater Gliders: Dynamics, Control, and Design," Ph.D. thesis, Princeton University, Princeton, NJ.
[6] Davis, R. E., Leonard, N. E., and Fratantoni, D. M., 2009, "Routing Strategies for Underwater Gliders," Deep Sea Res. Part II, **56**(3–5), pp. 173–187.
[7] Blidberg, D., 2001, "The Development of Autonomous Underwater Vehicles (AUV); A Brief Summary," IEEE International Conference on Robotics and Automation (ICRA), Seoul, South Korea, May 21–26.
[8] Smith, R., and Chao, Y., 2010, "Planning and Implementing Trajectories for Autonomous Underwater Vehicles to Track Evolving Ocean Processes Based on Predictions From a Regional Ocean Model," Int. J. Rob. Res., **29**(12), pp. 1475–1497.
[9] Mahmoudian, N., 2009, "Efficient Motion Planning and Control for Underwater Gliders," Ph.D. thesis, Virginia Polytechnic Institute and State University, Blacksburg, VA.
[10] Leonard, N. E., and Graver, J. G., 2001, "Model-Based Feedback Control of Autonomous Underwater Gliders," IEEE J. Oceanic Eng., **26**(4), pp. 633–645.
[11] Mahmoudian, N., and Woolsey, C. A., 2008, "Underwater Glider Motion Control," Proceedings of IEEE Conference on Decision and Control, Cancun, Mexico, Dec. 9–11, pp. 552–557.
[12] Bhatta, P., 2006, "Nonlinear Stability and Control of Gliding Vehicles," Ph.D. thesis, Princeton University, Princeton, NJ.
[13] Bhatta, P., and Leonard, N., 2008, "Nonlinear Gliding Stability and Control for Vehicles With Hydrodynamic Forcing," Automatica, **44**(5), pp. 1240–1250.
[14] Heidemann, J., Ye, W., Wills, J., Syed, A., and Li, Y., 2006, "Research Challenges and Applications for Underwater Sensor Networking," IEEE Wireless Communications and Networking Conference, Las Vegas, NV, Apr. 3–6, Vol. 1, pp. 228–235.
[15] Kinsey, J. C., Eustice, R. M., and Whitcomb, L. L., 2006, "A Survey of Underwater Vehicle Navigation: Recent Advances and New Challenges," IFAC Conference of Manoeuvering and Control of Marine Craft, Lisbon, Portugal. Sept. 20–22.
[16] Zhang, F., and Tan, X., 2013, "Gliding Robotic Fish and Its Tail-Enabled Yaw Motion Stabilization Using Sliding Mode Control," ASME Paper No. DSCC2013-4015.
[17] Zhang, F., Tan, X., and Khalil, H. K., 2012, "Passivity-Based Controller Design for Stabilization of Underwater Gliders," Proceedings of the 2012 American Control Conference, Montreal, QC, Canada, June 27–29, pp. 5408–5413.
[18] Khalil, H. K., 1987, "Stability Analysis of Nonlinear Multiparameter Singularly Perturbed Systems," IEEE American Control Conference, Minneapolis, MN, June 10–12, pp. 1219–1223.
[19] Khalil, H., 2002, *Nonlinear Systems*, Prentice Hall, Upper Saddle River, NJ.
[20] Kokotović, P., Khalil, H., and O'Reilly, J., 1999, *Singular Perturbation Methods in Control: Analysis and Design*, Society for Industrial and Applied Mathematics.
[21] Zhang, F., and Tan, X., 2014, "Nonlinear Observer Design for Stabilization of Gliding Robotic Fish," IEEE American Control Conference (ACC), Portland, OR, June 4–6, pp. 4715–4720.
[22] Zhang, F., Thon, J., Thon, C., and Tan, X., 2013, "Miniature Underwater Glider: Design and Experimental Results," IEEE/ASME Trans. Mechatronics, **19**(1), pp. 394–399.
[23] Zhang, F., Zhang, F., and Tan, X., 2012, "Steady Spiraling Motion of Gliding Robotic Fish," IEEE/RSJ International Conference on Intelligent Robots and Systems (IROS), Vilamoura, Portugal, Oct. 7–12, pp. 1754–1759.